Mechanism of Hydride-Ion Diffusion in the Oxyhydride of Barium Titanate

THE JOURNAL OF PHYSICAL CHEMISTRY C
A JOURNAL OF THE AMERICAN CHEMICAL SOCIETY

pubs.acs.org/JPCC
Article

Mechanism of Hydride-Ion Diffusion in the Oxyhydride of Barium Titanate

Rasmus Lavén, Lucas Fine, Elena Naumovska, Hua Guo, Ulrich Häussermann, Aleksander Jaworski, Masato Matsuura, Michael Marek Koza, and Maths Karlsson*

Cite This: J. Phys. Chem. C 2025, 129, 12305−12311
Read Online

ABSTRACT: Perovskite-type oxyhydrides stand out as hydride-ion conductors of relevance for diverse technological applications, but fundamental questions surrounding the relationship between the mechanism of hydride-ion diffusion and the local structure of these materials remain to be elucidated. Here, in a quasielastic neutron scattering (QENS) study of two perovskite-type oxyhydrides of barium titanate, $BaTiO_{2.67}H_{0.12}\square_{0.21}$ ($\square$ refers to anion vacancies) and $BaTiO_{2.88}H_{0.12}$, we establish that the mechanism of hydride-ion diffusivity relies on hydride-ion jumps to nearest-neighbor anion vacancies. Combined analyses of QENS and structural data for $BaTiO_{2.67}H_{0.12}\square_{0.21}$ show that the diffusion process is characterized by two different time scales, possibly related to diffusion in regions featured by different concentrations of anion vacancies. It follows that designing materials with specific concentrations of anion vacancies may be an effective route to optimize hydride-ion conductivity toward specific applications.

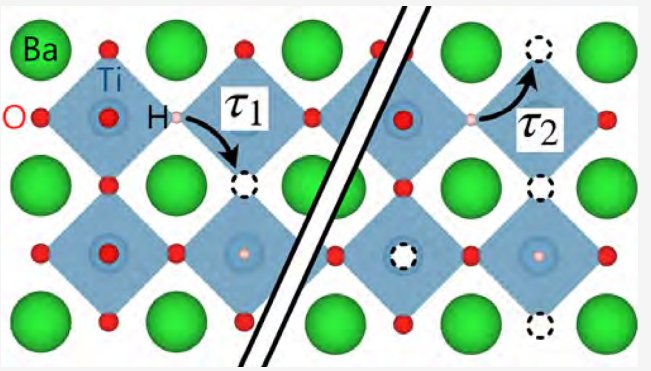

1. INTRODUCTION

Perovskite-type oxyhydrides of the form $ATiO_{3-x}H_x$ (A = Ba, Sr, and Ca; and $x < 0.6$) are a novel class of mixed-anion materials displaying high hydride-ion conductivity at elevated temperatures.[1−3] The hydride-ion conductivity may be exploited for applications in, e.g., energy storage and conversion, and in catalyst technologies for hydrogenation reactions.[4−7] However, despite several experimental studies, by solid-state nuclear magnetic resonance (NMR),[8] hydrogen/deuterium exchange,[9] and QENS,[10] as well as computer simulations,[9−12] a consensus regarding the nature of the mechanism of the hydride-ion diffusivity in these materials has not yet been reached. Specifically, QENS[10] and simulations[9,12] suggest hydride-ion jumps to both nearest- and next-nearest-neighbor anion vacancies, with a significantly lower activation energy for the former. In contrast, solid-state NMR[8] excludes nearest-neighbor jumps, reporting only jumps between next-nearest-neighbors, or that the nearest neighboring jumps happens on a much slower time scale of >1 ms. Hydrogen/deuterium exchange experiments indicate the coexistence of both jump types but yield activation energies 1 order of magnitude higher than QENS.[9] Additionally, some simulations propose an alternative interstitial diffusion mechanism.[11]

Recently, some of us reported on a QENS study on oxyhydrides of barium titanate characterized by the simultaneous presence of hydride ions and oxygen vacancies, i.e., $BaTiO_{3-x}H_y\square_{x-y}$, with $x = 0.18−0.7$ and $y = 0.04−0.1$.[10] The results of this study unveiled the presence of a highly temperature-dependent diffusion mechanism. For T = 225 and 250 K, the diffusion mechanism was found to be characterized by hydride-ion jumps between nearest-neighbor anion vacancies, with a mean residence time of the order of 0.1 ns, whereas for $T > 400$ K, it was found to be characterized by the (exclusive or additional) presence of hydride-ion jumps between next-nearest-neighbor anion vacancies.[10] A diffusion coefficient was extracted from the QENS data and was found to take on values of about 0.4×10^{-6} cm^2 s^{-1} at 225 K and between ca. 20×10^{-6} and 100×10^{-6} cm^2 s^{-1} at temperatures between 400 and 700 K. Activation energies were derived from the measurements at high temperatures and take on values of about 0.1 eV, with a slight increase with increasing anion vacancy concentration.

To establish whether hydride-ion diffusion occurs solely through a vacancy-assisted jump-diffusion process, and whether the nature of the jumps, e.g., the jump length, depends on the concentration of hydride-ion and anion vacancies, a systematic investigation of samples differing in

Received: April 3, 2025
Revised: June 6, 2025
Accepted: June 17, 2025
Published: June 28, 2025

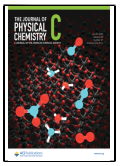

anion vacancy concentrations, including a sample with virtually no, other than thermodynamically formed, anion vacancies, is needed. In this work, we thus investigate the nature of hydride-ion diffusion in two samples of the oxyhydride of barium titanate, one of which is characterized by a relatively large concentration of anion vacancies, i.e., $BaTiO_{2.67}H_{0.12}\square_{0.21}$, and one virtually free of anion vacancies, $BaTiO_{2.88}H_{0.12}$, using QENS. The aim of the study is two-fold: first, to elucidate whether hydride-ion diffusion occurs solely through a vacancy-assisted jump-diffusion process, and second, to determine the mechanistic details, such as the time scale, activation energy, and spatial geometry, of the diffusion process.

2. EXPERIMENTAL DETAILS

The samples, $BaTiO_{2.67}H_{0.12}\square_{0.21}$ and $BaTiO_{2.88}H_{0.12}$, were synthesized and characterized according to the procedure described in refs 13 and 14. For comparison, we also investigated the sample $BaTiO_{2.65}H_{0.08}\square_{0.27}$ (CA2), which was investigated in our previous QENS study.[10] Details of the sample synthesis and the characterization of the samples' structural and chemical properties are provided in the Supporting Information (SI).

The QENS experiments were performed on three different instruments, namely, the backscattering spectrometer DNA at the Japan Proton Accelerator Research Complex (J-PARC),[15] and the backscattering spectrometer IN16B[16] and the time-of-flight spectrometer IN5[17] at the Institut Laue-Langevin in France.

The experiment on DNA focused on measurements of $BaTiO_{2.67}H_{0.12}\square_{0.21}$ and $BaTiO_{2.65}H_{0.08}\square_{0.27}$ (CA2). For $BaTiO_{2.67}H_{0.12}\square_{0.21}$, measurements were performed at the temperatures T = 5, 250, 300, 350, 400, 450, 500, and 550 K, in that order, whereas for CA2, measurements were taken at T = 300 K. The samples, approximately 5 g per composition, were filled into cylindrically shaped sample cells of aluminum that were subsequently sealed by steel wires. The instrument was set up using Si(111) crystal analyzers, which give access to a momentum transfer (q) range of 0.3−1.8 Å^{-1}, and without and with a pulse-shaping chopper. Without the pulse-shaping chopper (low-resolution (LR) setup), the energy resolution is about 10 μeV at full width at half-maximum (FWHM) at the elastic line, which gives access to an energy transfer (E) range of −500 to 1000 μeV. With the pulse-shaping chopper (high-resolution (HR) setup), the energy resolution is increased to 3.5 μeV at FWHM at the elastic line, which gives access to an E range of −40 to 50 μeV.

The experiment on IN16B and IN5 focused on measurements of the sample of composition $BaTiO_{2.88}H_{0.12}$, i.e., the sample virtually free of anion vacancies. The combination of both instruments IN16B and IN5 allowed us to probe similar time scales and distances as for the experiment at DNA, i.e., ≈1−500 ps and ≈3−30 Å, respectively, thus making the measurements comparable. The measurements were performed at T = 50, 100, 250, 300, 350, 400, 450, 500, and 550 K on IN5 and at T = 2, 225, 250, 275, and 325 K on IN16B. IN16B was used in its high-flux setup with the Si(111) crystal analyzers, which gives access to an energy resolution of 0.8 μeV at FWHM at the elastic lines and E and q ranges of −30 to 30 μeV and 0.2−1.8 Å^{-1}, respectively. IN5 was used with 5 Å incident wavelength neutrons, which gives access to an energy resolution of 100 μeV at FWHM at the elastic line, a maximum energy transfer of 2 meV, and a q-range of 0.2−2.2 Å^{-1}.

In all experiments, the data reduction included normalization of the detectors using a vanadium standard, and measurements on DNA and IN5 required a transformation from time-of-flight and scattering angle to E and q. The obtained quantity is the dynamic structure factor, $S(q, E)$, which expresses the scattering intensity as a function of q and E.

3. RESULTS

3.1. Fast-Time Scale Diffusion (LR Setup). Measurements of relatively fast-time scale diffusion were performed using the LR setup of DNA. First, we discuss the results obtained for $BaTiO_{2.67}H_{0.12}\square_{0.21}$. Figure 1a shows $S(E)$, the dynamical structure factor summed over the whole measured q-range (0.3−1.8 Å^{-1}), as a function of temperature. As can be seen, there is a quasielastic signal observed for T > 250 K, which can be ascribed to hydride-ion diffusion being activated on the accessible time scale of the instrument, as previously assigned for CA2.[10] The maximum intensity of the elastic peak (shown as an inset) decreases with increasing quasielastic scattering intensity, as expected. For all measured temperatures and q-values, the $S(q, E)$ could be adequately fitted to a function of the form

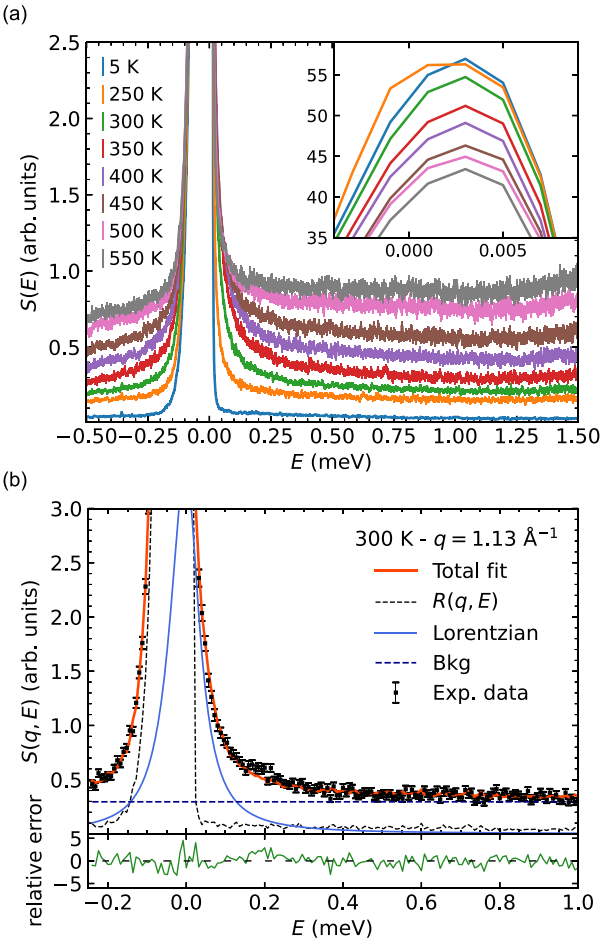

Figure 1. QENS data for $BaTiO_{2.67}H_{0.12}\square_{0.21}$, as measured on DNA with the LR setup. (a) $S(E)$ for different temperatures. Inset shows a close-up of the maximum intensity of the elastic peak. (b) $S(q, E)$ for q = 1.13 Å^{-1} as measured at 300 K. The relative error is calculated as (data - fit)/(error on data).

https://doi.org/10.1021/acs.jpcc.5c02250
J. Phys. Chem. C 2025, 129, 12305−12311

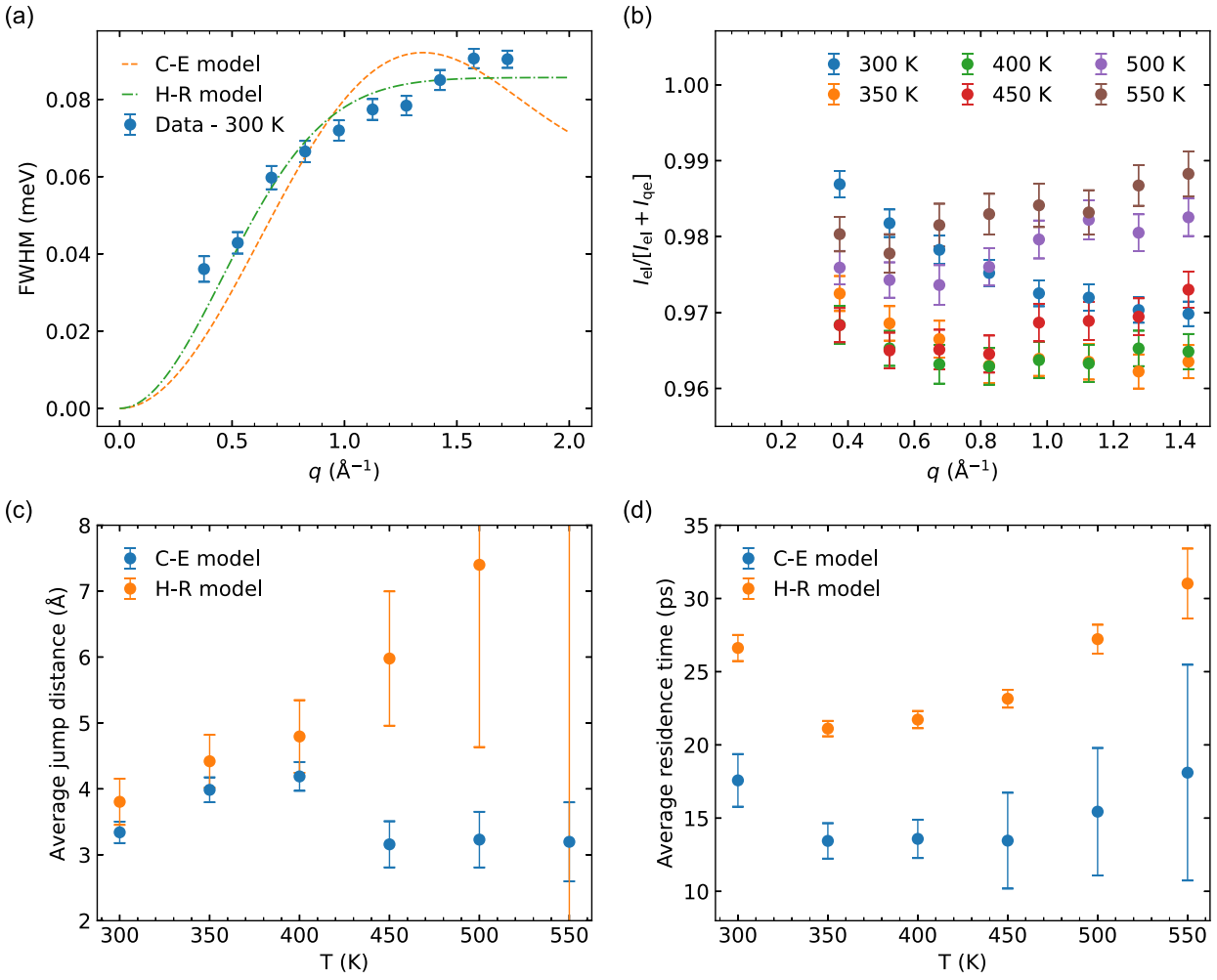

Figure 2. QENS data and fitting results for $BaTiO_{2.67}H_{0.12}\square_{0.21}$. The data were measured on DNA with the LR setup. (a) Quasielastic line width (FWHM) plotted as a function of q at 300 K, together with fits to the Chudley−Elliot (C−E) and Hall−Ross (H−R) models of jump diffusion. (b) Elastic fraction plotted as a function of q, for different temperatures. (c) Average jump distances (the average jump distance at 550 K for the H−R model is ≈9 Å) and (d) average residence time, τ, as a function of temperature.

$$S(q, E) = [I_{el}(q)\delta(E) + I_{qe}(q)\mathcal{L}(E; q)] \otimes R(q, E) + \mathrm{Bkg}(q) \quad (1)$$

where $I_{el}(q)$ and $I_{qe}(q)$ are the elastic and quasielastic intensities, respectively, and $\mathcal{L}(E; q)$ is a Lorentzian function with a q-dependent line width (FWHM) that describes the quasielastic scattering. $\delta(E)$ is a Dirac delta function, which describes the elastic scattering, $R(q, E)$ is the instrumental resolution function, and $\mathrm{Bkg}(q)$ is a background function. Figure 1b shows, as an example, $S(q, E)$ at q = 1.13 Å^{-1} as measured at 300 K, together with the fit according to eq 1. It should be noted that a single Lorentzian component provided a satisfactory fit of the data. Fits for additional q-values are shown in Figure S4.

Our more detailed analysis of the quasielastic scattering shows that the line width (FWHM) of the Lorentzian component increases as a function of increasing q (see Figure 2a for data at 300 K, and the data for all temperatures in Figure S5), whereas the relative intensity of the elastic scattering $[I_{el}/(I_{el} + I_{qe})]$ is approximately q-independent (Figure 2b). The observed q-dependence of the quasielastic line width and elastic intensity both suggest that the diffusion is of long-range character.

Included in Figure 2a are free fits to the Chudley−Elliott (C−E) and Hall−Ross (H−R) models of jump diffusion. The C−E model describes diffusion on a perfect lattice, characterized by a fixed jump length,[18] while the H-R model is characterized by a Gaussian distribution of jump lengths, which could reflect diffusion in a structurally disordered material.[19] As can be seen, both models fit reasonably well to the data, with the average jump distances for each model shown in Figure 2c. For both models, the jump distances increase with temperature, from about d = 3.3 Å at 300 K to d = 4.2 Å at 400 K, suggesting that the average jump length can be robustly estimated without taking into account the geometrical details of the jump-diffusion mechanism. Crucially, these average jump distances are similar to the distances between nearest-neighbor (2.8 Å) and next-nearest-neighbor (4.0 Å) anion sites in $BaTiO_{2.67}H_{0.12}\square_{0.21}$, which suggests that there is a progression from predominantly nearest-neighbor jumps at 300 K to predominantly next-nearest-neighbor jumps at 350 and 400 K. For higher temperatures, however, the average jump distances as extracted from the two fitting models depart and are featured by a larger error. Possibly, this is a result of a higher background in the $S(q, E)$ at these higher temperatures, which makes the fitting results less reliable. The reason for this large background is at present unclear, but we

https://doi.org/10.1021/acs.jpcc.5c02250
J. Phys. Chem. C 2025, 129, 12305−12311

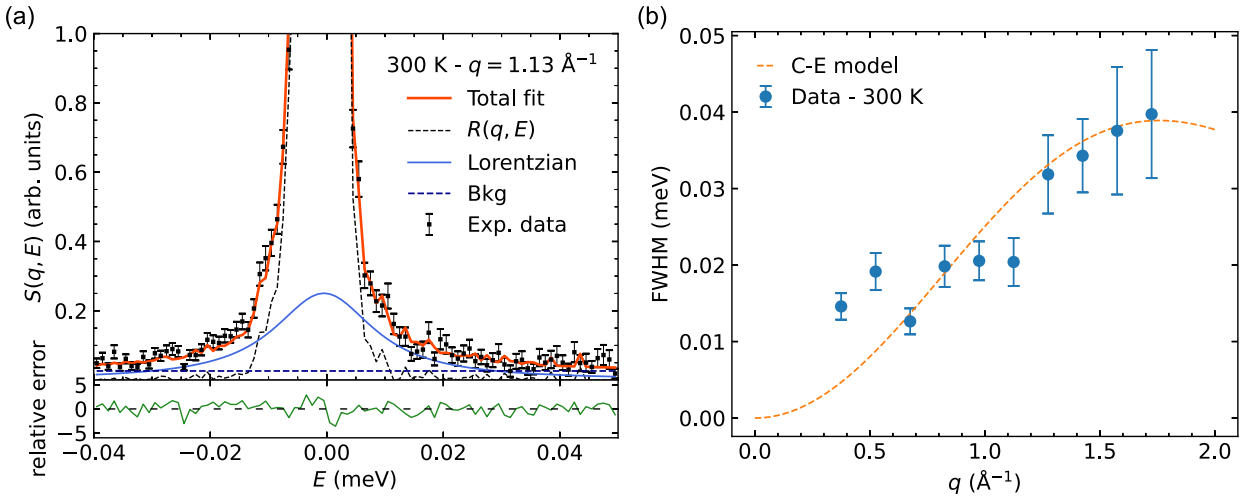

Figure 3. QENS data and fitting results for $BaTiO_{2.67}H_{0.12}\square_{0.21}$. The data were measured on DNA with the HR setup. (a) $S(q, E)$ together with a fit at 300 K and q = 1.13 Å^{-1}. (b) FWHM at 300 K together with a fit to the C−E model.

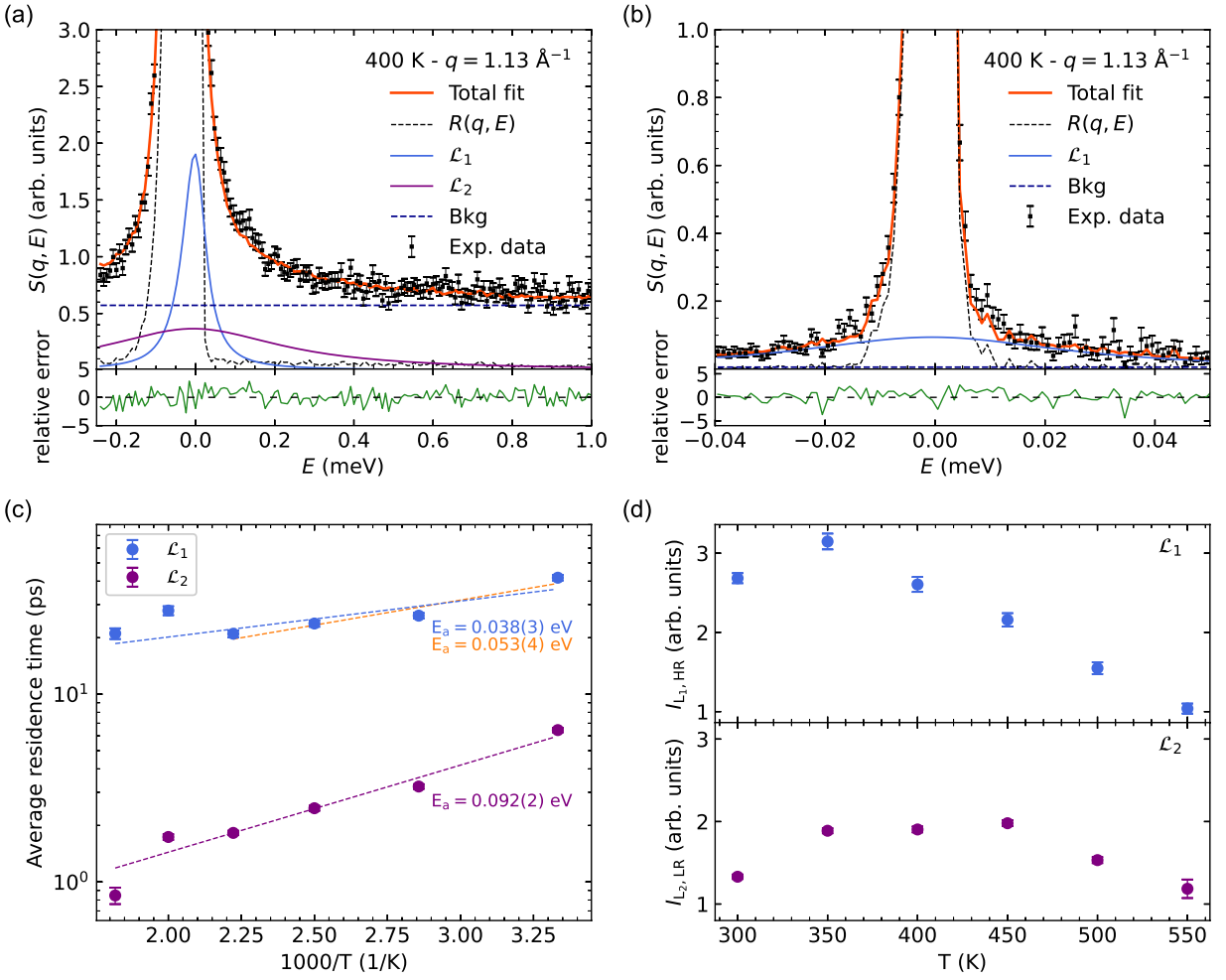

Figure 4. QENS data and fitting results for the combined analysis for $BaTiO_{2.67}H_{0.12}\square_{0.21}$. (a) $S(q, E)$ as measured with the LR setup at 400 K and q = 1.13 Å^{-1}, together with fit. (b) $S(q, E)$ as measured with the HR setup at 400 K and q = 1.13 Å^{-1}, together with fit. (c) Average residence time as a function of temperature, together with fits to an Arrhenius law. The apparent activation energies, as extracted from the fit, are indicated. For the slower Lorentzian, the orange line takes into account only the data points for $T \leq 450$ K, whereas the blue line takes into account all data points. (d) Amplitude of the Lorentzian components as a function of temperature.

note that a similar background was observed in the study by Eklöf-Österberg et al.[10] and might indicate additional, faster-time scale diffusion in the material that is too fast to be observed on the time window of DNA.

https://doi.org/10.1021/acs.jpcc.5c02250
J. Phys. Chem. C 2025, 129, 12305−12311

The average residence time τ between two successive jumps can be extracted from the line width of the quasielastic component and is in the range of 10−30 ps, with a slight increase with temperature from 350 to 500 K for both models, as shown in Figure 2d. The average residence time at 300 K is featured by a relatively high value and does not follow the same trend. Because of the relatively weak quasielastic scattering intensity at this temperature, we consider it to be less reliable. Furthermore, a diffusion coefficient can be extracted from the data by taking $D = d^2/6\tau$.[21] It takes on values on the order of 10^{-5} cm^2 s^{-1} and varies slightly with temperature.

3.2. Slow-Time Scale Diffusion (HR Setup). Measurements of slower-time scale diffusion were realized using the HR setup on DNA. Figure 3a shows $S(q, E)$ for $BaTiO_{2.67}H_{0.12}\square_{0.21}$, as measured at q = 1.13 Å^{-1} and 300 K; data for all temperatures are shown in Figure S6. For all measured temperatures, the QENS spectra reveal pronounced quasielastic scattering, which can be adequately fitted to eq 1. Similarly to the faster-time scale diffusion as measured with the LR setup, the line width (FWHM) of the quasielastic scattering shows a systematic increase with increasing q and can be reasonably well fitted to a C-E model of jump diffusion, with an average jump length of about 2.6 Å (Figure 3b). This average jump length is similar to the distance between nearest neighbors (2.8 Å), which, hence, together with the analysis of the LR data, suggests the simultaneous presence of two long-range diffusion mechanisms of the hydride ions, exhibiting very similar geometrical behavior (jump length) but featured by different time scales. However, the above analyses are based on independent line shape fitting analyses of two sets of measurements with slightly overlapping dynamic ranges. This means that the slower-time scale diffusion may interfere with the fitting of the faster-time scale diffusion in the LR data and vice versa, thus affecting the fitting results. Indeed, the individual analyses of the QENS data result in a quite nonsystematic behavior in both the temperature dependence of the average residence time and the average jump distance for both jump-diffusion models, which suggest that the analyses are not robust over the whole temperature range.

3.3. Combined Analysis. To increase the robustness of the fitting parameters, especially in regard to the temperature dependence of the average residence time and jump distance, we performed a separate combined analysis of the QENS data. In this analysis, the HR data were fitted to the following function:

$$S(q, E)_{HR} = [I_{e1,HR}(q)\delta(E) + I_{L1,HR}\mathcal{L}_1(E; q)] \otimes R_{HR}(q, E) + Bkg_{HR}(q) \quad (2)$$

where $I_{L1,HR}$ is a q-independent scaling factor, and $\mathcal{L}_1$ is constrained to follow a q-dependence according to the C−E model, with a fixed jump distance of d = 2.8 Å. Thereafter, the LR data were fitted according to the following function:

$$S(q, E)_{LR} = [I_{el,LR}(q)\delta(E) + I_{L1,LR}\mathcal{L}_1(E; q) + I_{L2,LR}\mathcal{L}_2(E)] \otimes R_{LR}(q, E) + Bkg_{LR}(q) \quad (3)$$

Here, $\mathcal{L}_1$ is fixed from the fit to the HR data, $\mathcal{L}_2$ is constrained to follow a q-dependence according to the C−E model with a fixed jump distance of d = 2.8 Å, and $I_{L1,LR}$, and $I_{L2,LR}$ are q-independent scaling factors. The two Lorentzian functions, $\mathcal{L}_1$ and $\mathcal{L}_2$, thus describe the slower- and faster-time scale diffusion processes, respectively, and were both globally fitted with their FWHM fixed to a C−E model with jump distance of 2.8 Å.

Our combined analysis shows that $S(q, E)$ can be adequately fitted up to 550 K and, crucially, the temperature dependence of the obtained average residence time is more robust (see Figures 4c, S7 and S8) as compared with the independent fitting analyses. The average residence times are in the range of 20−40 and 2−6 ps, respectively, and decrease with increasing temperature. Self-diffusion coefficients can be extracted from these data, and these are on the order of 10^{-6} and 10^{-5} cm^2 s^{-1} for the slower and faster diffusion processes, respectively. The average residence time for the faster diffusion fits reasonably well to an Arrhenius temperature dependence, with an activation energy of 92(2) meV (Figure 4c).

These results align well with the activation energies of 85(2) meV and 94(2) meV previously measured for $BaTiO_{2.65}H_{0.08}\square_{0.27}$ (CA2) and $BaTiO_{2.3}H_{0.04}\square_{0.66}$, respectively,[10] confirming that similar dynamics are probed in both studies. However, one should note that the activation energy reported in ref 10 is obtained using a free fitting approach, whereas here it is obtained from the combined analysis using constrained global fitting, which may somewhat compromise the comparability of the results. Furthermore, additional measurements on $BaTiO_{2.65}H_{0.08}\square_{0.27}$ (CA2) using the HR and LR setups on DNA (see Figure S9) support this, revealing comparable time scales for diffusion in both samples. Specifically, at 300 K, the residence time for the slower diffusion is 34(1) ps in $BaTiO_{2.65}H_{0.08}\square_{0.27}$ and 42(1) ps in $BaTiO_{2.67}H_{0.12}\square_{0.21}$, while for the faster diffusion, it ranges from 1.9(1) to 6.4(2) ps, respectively.

Finally, one should note that the scaling factors of the Lorentzian components $I_{L1,HR}$ and $I_{L2,LR}$ (Figure 4d) reflect the amount of hydride ions that undergo these diffusion processes. As can be seen, there is a decreasing number of hydride ions undergoing the slower diffusion process with increasing temperature, whereas the number of hydride ions undergoing the faster diffusion process increases up to around 450 K. It should be noted that the drop of $I_{L2,LR}$ at 500 K is not reliable due to the high background at this temperature hampering the fitting analysis. This observation may indicate that a portion of the hydride ions undergoing slower diffusion at low temperatures undergo faster diffusion at high temperatures.

4. DISCUSSION

A key finding in our analysis is the coexistence of two different jump-diffusion processes, which are featured by the same average jump distance but different time scales of diffusion. We speculate that the different time scales may reflect that the respective diffusion processes occur in different local structures of the material, such as in regions of relatively high or low anion vacancy concentration, respectively. This idea is supported by our analysis of the PXRD data (see Figure S1 and Table S1), which revealed two slightly different cubic phases of the material, which may be characterized by different concentrations of anion vacancies.

In comparison to the QENS literature on related oxyhydrides, we note that the faster diffusion process observed in our study is similar to what was observed for $LaSrCoO_3H_{0.7}$,[22] whereas the slower one is similar to that observed for $SrVO_2H$.[23] As $LaSrCoO_3H_{0.7}$ is featured by a relatively high amount of anion vacancies,[22] whereas $SrVO_2H$ is believed to

https://doi.org/10.1021/acs.jpcc.5c02250
J. Phys. Chem. C 2025, 129, 12305−12311

be nearly stoichiometric in H and thus contains a low amount of anion vacancies,[24] this is in agreement with our observation of that the rate of hydride-ion diffusion appears to increase with increasing concentration of anion vacancies. Furthermore, our QENS measurements on the sample virtually free of anion vacancies, $BaTiO_{2.88}H_{0.12}$, indeed did not show any significant sign of quasielastic scattering for temperatures up to as high as 550 K (see Figures S10 and S11 for T = 300−550 K), suggesting that the presence of a significant amount of anion vacancies is a necessity for hydride-ion diffusion in oxyhydrides of barium titanate and, most likely, also in many other oxyhydrides.

It should be noted that the diffusion coefficient extracted from our QENS measurements is several orders of magnitude larger than what has been observed using more macroscopic techniques. For example, Liu et al.[25] measured the diffusion coefficients in thin films of $SrTiO_{3-x}H_x$ using secondary ion mass spectroscopy depth profiling with isotope exchange. They reported a diffusion coefficient on the order of 10^{-13} cm^2/s, which is several orders of magnitude lower than what we observe using QENS. Their analysis yields a diffusion coefficient for diffusion through the whole thin film with a thickness of about 80 nm and will thus also depend on grain boundaries and other defects. For QENS, one should probe, in principle, the pure bulk self-diffusion coefficient. However, QENS probes significantly smaller length scales. The largest length scale probed in our experiment can be roughly estimated from the lowest measured q value by $2\pi/q_{min} \approx 17$ Å. This corresponds to a length of about four unit cells, and it is possible that diffusion on a longer length scale is significantly slower than what we observe here; i.e., we cannot exclude that the observed motion becomes quasi-localized on longer length scales. In comparison, the 80 nm distance probed in the study of Liu et al.[25] corresponds to about 200 unit cells, which might relate to the discrepancy in the results. It should also be noted that, in our experiment, most scattering is observed to be purely elastic, with the quasielastic signal being only a few percent of the total scattering intensity. This means that only a few percent of the hydride ions undergo dynamics that can be observed on the here probed time scales. This supports that these mobile hydride ions relate to specific local environments in the material, possibly related to regions relatively rich in anion vacancies that could be found, for example, in the vicinity of grain boundaries and/or other types of defects in the material.

Further insight into the nature of hydride-ion diffusivity comes by comparing the experimentally determined activation energy of 92(2) meV with theoretical values from simulations.[12,26] Notably, the activation energy increases to 830 meV in the presence of electron polarons near Ti atoms, compared to 290 meV in their absence.[26] Therefore, the low activation energy observed in our sample suggests a negligible concentration of electron polarons. Together, the QENS data and simulations highlight two key design principles for enhancing hydride-ion mobility: (i) maintaining an anion vacancy concentration higher than that of hydride ions and (ii) suppressing electron polaron formation, e.g., through bandgap engineering to reduce the activation barrier.

We end with a caveat in that $BaTiO_{2.88}H_{0.12}$ is featured by a significantly smaller amount of surface −OH groups and adsorbed H_2O species (see Figure S3). Thus, it cannot be excluded that the quasielastic signal (whole or in part) for $BaTiO_{2.67}H_{0.12}\square_{0.21}$ originates from the dynamics of such species, rather than from hydride ions in the bulk of the material. While adsorbed H_2O would most likely not be present at 550 K (where we still observe dynamics), a recent study showed evidence of significant surface alterations of barium titanate oxyhydrides when using LiH as a reducing agent for T > 400 °C, giving rise to surface layers of $TiO_x(OH)$.[14] We cannot exclude that the hydrogen dynamics probed with QENS relate to dynamics in such surface layers, although we also note that inelastic neutron scattering shows no evidence for the presence of such species.[20]

5. CONCLUSIONS

To conclude, our QENS study of oxyhydrides of barium titanate establishes that the mechanism of hydride-ion diffusivity relies on hydride-ion jumps to nearest-neighbor anion vacancies and, therefore, that the presence of anion vacancies is a strict necessity for hydride-ion diffusion. Crucially, the combined analysis of QENS and structural data for $BaTiO_{2.67}H_{0.12}\square_{0.21}$ shows that the diffusion process is characterized by two different time scales. We hypothesize that the faster process occurs in regions featured by a relatively high amount of anion vacancies, and the slower diffusion process happens in regions featured by a relatively low amount of anion vacancies. Designing materials with specific concentrations of anion vacancies—e.g., by using LiH as a reducing agent and varying the synthesis temperature, as have been reported recently[14]—may thus be effective in optimizing the level of hydride-ion conductivity, with a view toward specific applications.

■ ASSOCIATED CONTENT

Supporting Information

The Supporting Information is available free of charge at https://pubs.acs.org/doi/10.1021/acs.jpcc.5c02250.

Details of the sample synthesis, PXRD, TG, and NMR data; additional QENS data and analysis for $BaTiO_{2.67}H_{0.12}\square_{0.21}$; QENS data on CA2; and QENS data on $BaTiO_{2.88}H_{0.12}$ (PDF)

■ AUTHOR INFORMATION

Corresponding Author

Maths Karlsson − *Department of Chemistry and Chemical Engineering, Chalmers University of Technology, Göteborg 41296, Sweden;* orcid.org/0000-0002-2914-6332; Email: maths.karlsson@chalmers.se

Authors

Rasmus Lavén − *Department of Chemistry and Chemical Engineering, Chalmers University of Technology, Göteborg 41296, Sweden;* orcid.org/0000-0001-8165-461X

Lucas Fine − *Department of Chemistry and Chemical Engineering, Chalmers University of Technology, Göteborg 41296, Sweden; Institut Laue-Langevin, Grenoble 38042, France;* orcid.org/0000-0003-2755-1980

Elena Naumovska − *Department of Chemistry and Chemical Engineering, Chalmers University of Technology, Göteborg 41296, Sweden;* orcid.org/0000-0001-6011-5369

Hua Guo − *Department of Materials and Environmental Chemistry, Stockholm University, Stockholm 10691, Sweden*

Ulrich Häussermann − *Department of Materials and Environmental Chemistry, Stockholm University, Stockholm 10691, Sweden;* orcid.org/0000-0003-2001-4410

Aleksander Jaworski − *Department of Materials and Environmental Chemistry, Stockholm University, Stockholm 10691, Sweden;* orcid.org/0000-0002-7156-559X
Masato Matsuura − *Comprehensive Research Organization for Science and Society, Naka-gun 319-1106, Japan*
Michael Marek Koza − *Institut Laue-Langevin, Grenoble 38042, France;* orcid.org/0000-0002-5133-8584

Complete contact information is available at: https://pubs.acs.org/10.1021/acs.jpcc.5c02250

Notes

The authors declare no competing financial interest.

■ ACKNOWLEDGMENTS

M.K. is thankful for support from the Swedish Research Council (Grant Nos. 2014-03980, 2016-06958, and 2021-04807) and the Swedish Energy Agency (Grant No. 48712-1), and the Institut Laue-Langevin (Grant No. ILL-1880.1). U.H. is thankful for support from the Swedish Research Council (Grant No. 2014-03980). Furthermore, we are thankful to Michael Sannemo Targama at Stockholm University for help with the Rietveld analysis and to Markus Appel at the ILL for help during the IN16B measurements. The neutron experiment at the Materials and Life Science Experimental Facility of the J-PARC was performed under a user program (Proposal 2019B0050). The neutron experiment at the Institut Laue-Langevin was performed under a user program (DOI: 10.5291/ILL-DATA.7-03-206).

■ REFERENCES

(1) Kobayashi, Y.; Hernandez, O. J.; Sakaguchi, T.; Yajima, T.; Roisnel, T.; Tsujimoto, Y.; Morita, M.; Noda, Y.; Mogami, Y.; Kitada, A.; et al. An oxyhydride of $BaTiO_3$ exhibiting hydride exchange and electronic conductivity. *Nat. Mater.* **2012**, *11*, 507−511.
(2) Yajima, T.; Kitada, A.; Kobayashi, Y.; Sakaguchi, T.; Bouilly, G.; Kasahara, S.; Terashima, T.; Takano, M.; Kageyama, H. Epitaxial thin films of $ATiO_{3-x}H_x$ (A = Ba, Sr, Ca) with metallic conductivity. *J. Am. Chem. Soc.* **2012**, *134*, 8782−8785.
(3) Sakaguchi, T.; Kobayashi, Y.; Yajima, T.; Ohkura, M.; Tassel, C.; Takeiri, F.; Mitsuoka, S.; Ohkubo, H.; Yamamoto, T.; Kim, J. E.; et al. Oxyhydrides of $(Ca,Sr,Ba)TiO_3$ Perovskite Solid Solutions. *Inorg. Chem.* **2012**, *51*, 11371−11376.
(4) Kitano, M.; Inoue, Y.; Ishikawa, H.; Yamagata, K.; Nakao, T.; Tada, T.; Matsuishi, S.; Yokoyama, T.; Hara, M.; Hosono, H. Essential role of hydride ion in ruthenium-based ammonia synthesis catalysts. *Chem. Sci.* **2016**, *7*, 4036−4043.
(5) Tang, Y.; Kobayashi, Y.; Masuda, N.; Uchida, Y.; Okamoto, H.; Kageyama, T.; Hosokawa, S.; Loyer, F.; Mitsuhara, K.; Yamanaka, K.; et al. Metal-Dependent Support Effects of Oxyhydride-Supported Ru, Fe, Co Catalysts for Ammonia Synthesis. *Adv. Energy Mater.* **2018**, *8*, No. 1801772.
(6) Kobayashi, G.; Hinuma, Y.; Matsuoka, S.; Watanabe, A.; Iqbal, M.; Hirayama, M.; Yonemura, M.; Kamiyama, T.; Tanaka, I.; Kanno, R. Pure H^- conduction in oxyhydrides. *Science* **2016**, *351*, 1314−1317.
(7) Irvine, J. T.; Wilson, S.; Amnuaypanich, S.; Irvine, G. J.; Verbraeken, M. C.; Nowicki, K.; Carins, G. M. Hydrogen ionic conductors and ammonia conversions. *Farad. Disc.* **2023**, *243*, 296−306.
(8) Aleksis, R.; Nedumkandathil, R.; Papawassiliou, W.; Carvalho, J. P.; Jaworski, A.; Häussermann, U.; Pell, A. J. Probing the electronic structure and hydride occupancy in barium titanium oxyhydride through DFT-assisted solid-state NMR. *Phys. Chem. Chem. Phys.* **2022**, *24*, 28164−28173.
(9) Tang, Y.; Kobayashi, Y.; Shitara, K.; Konishi, A.; Kuwabara, A.; Nakashima, T.; Tassel, C.; Yamamoto, T.; Kageyama, H. On Hydride Diffusion in Transition Metal Perovskite Oxyhydrides Investigated via Deuterium Exchange. *Chem. Mater.* **2017**, *29*, 8187−8194.
(10) Eklöf-Österberg, C.; Nedumkandathil, R.; Häussermann, U.; Jaworski, A.; Pell, A. J.; Tyagi, M.; Jalarvo, N. H.; Frick, B.; Faraone, A.; Karlsson, M. Dynamics of Hydride Ions in Metal Hydride-Reduced $BaTiO_3$ Samples Investigated with Quasielastic Neutron Scattering. *J. Phys. Chem. C* **2019**, *123*, 2019−2030.
(11) Zhang, J.; Gou, G.; Pan, B. Study of Phase Stability and Hydride Diffusion Mechanism of $BaTiO_3$ Oxyhydride from First-Principles. *J. Phys. Chem. C* **2014**, *118*, 17254−17259.
(12) Liu, X.; Bjørheim, T. S.; Haugsrud, R. Formation and migration of hydride ions in $BaTiO_{3-x}H_x$ oxyhydride. *J. Mater. Chem. A* **2017**, *5*, 1050−1056.
(13) Nedumkandathil, R.; Jaworski, A.; Grins, J.; Bernin, D.; Karlsson, M.; Eklöf-Österberg, C.; Neagu, A.; Tai, C. W.; Pell, A. J.; Häussermann, U. Hydride Reduction of $BaTiO_3$−Oxyhydride Versus O Vacancy Formation. *ACS Omega* **2018**, *3*, 11426−11438.
(14) Guo, H.; Jaworski, A.; Ma, Z.; Slabon, A.; Bacsik, Z.; Nedumkandathil, R.; Häussermann, U. Trapping of different stages of $BaTiO_3$ reduction with LiH. *RSC Adv.* **2020**, *10*, 35356−35365.
(15) Shibata, K.; Takahashi, N.; Kawakita, Y.; Matsuura, M.; Yamada, T.; Tominaga, T.; Kambara, W.; Kobayashi, M.; Inamura, Y.; Nakatani, T.et al.The Performance of TOF near Backscattering Spectrometer DNA in MLF, J-PARC. In *Proceedings of the 2nd International Symposium on Science at J-PARC. Unlocking the Mysteries of Life, Matter and the Universe. J. Phys. Soc. Japan*; **2015**; Vol. *8*, p 036022.
(16) Frick, B.; Mamontov, E.; van Eijck, L.; Seydel, T. Recent Backscattering Instrument Developments at the ILL and SNS. *Z. Phys. Chem.* **2010**, *224*, 33−60.
(17) Ollivier, J.; Mutka, H. IN5 Cold Neutron Time-of-Flight Spectrometer, Prepared to Tackle Single Crystal Spectroscopy. *J. Phys. Soc. Jpn.* **2011**, *80*, SB003.
(18) Chudley, C. T.; Elliott, R. J. Neutron Scattering from a Liquid on a Jump Diffusion Model. *Proc. Phys. Soc.* **1961**, *77*, 353−361.
(19) Hall, P. L.; Ross, D. K. Incoherent neutron scattering functions for random jump diffusion in bounded and infinite media. *Mol. Phys.* **1981**, *42*, 673−682.
(20) Eklöf-Österberg, C.; Mazzei, L.; Granhed, E. J.; Wahnström, G.; Nedumkandathil, R.; Häussermann, U.; Jaworski, A.; Pell, A. J.; Parker, S. F.; Jalarvo, N. H.; et al. The role of oxygen vacancies on the vibrational motions of hydride ions in the oxyhydride of barium titanate. *J. Mater. Chem. A* **2020**, *8*, 6360−6371.
(21) Hempelmann, R. *Quasielastic Neutron Scattering and Solid State Diffusion*; Oxford University Press: 2000.
(22) Bridges, C. A.; Fernandez-Alonso, F.; Goff, J. P.; Rosseinsky, M. J. Observation of hydride mobility in the transition-metal oxide hydride $LaSrCoO_3H_{0.7}$. *Adv. Mater.* **2006**, *18*, 3304−3308.
(23) Lavén, R.; Häussermann, U.; Perrichon, A.; Andersson, M. S.; Targama, M. S.; Demmel, F.; Karlsson, M. Diffusional Dynamics of Hydride Ions in the Layered Oxyhydride $SrVO_2H$. *Chem. Mater.* **2021**, *33*, 2967−2975.
(24) Denis Romero, F.; Leach, A.; Möller, J. S.; Foronda, F.; Blundell, S. J.; Hayward, M. A. Strontium vanadium oxide-hydrides: "Square-Planar" Two-Electron Phases. *Angew. Chemie - Int. Ed.* **2014**, *53*, 7556−7559.
(25) Liu, X.; Bjørheim, T. S.; Vines, L.; Fjellvåg, Ø. S.; Granerød, C.; Prytz, Ø.; Yamamoto, T.; Kageyama, H.; Norby, T.; Haugsrud, R. Highly Correlated Hydride Ion Tracer Diffusion in $SrTiO_{3-x}H_x$ Oxyhydrides. *J. Am. Chem. Soc.* **2019**, *141*, 4653−4659.
(26) Fine, L.; Karlsson, M.; Panas, I.; Koza, M. M. Unraveling the Electronic Control of Hydride Diffusivity in Oxyhydrides from Model Studies on $BaTiO_{3-x}H_y$. Unpublished, 2025.